Sedimentary Geology 373 (2018) 98–110

Contents lists available at ScienceDirect

Sedimentary Geology

journal homepage: www.elsevier.com/locate/sedgeo

Pedogenic record of climate change across the Pennsylvanian-Permian boundary in red-bed strata of the Cutler Group, northern New Mexico, USA

Lawrence H. Tanner [a,*], Spencer G. Lucas [b]

[a] Department of Biological & Environmental Sciences, Le Moyne College, Syracuse, NY 13214, USA
[b] New Mexico Museum of Natural History, 1801 Mountain Road N.W., Albuquerque, NM 87014, USA

ARTICLE INFO

Article history:
Received 10 April 2018
Received in revised form 24 May 2018
Accepted 25 May 2018
Available online 30 May 2018

Editor: Dr. B. Jones

Keywords:
Virgilian
Wolfcampian
Paleoclimate
Aridification
Monsoon
Calcrete

ABSTRACT

The Upper Pennsylvanian to lowermost Permian El Cobre Canyon and Arroyo del Agua formations are well exposed in a 250+ m section in the Chama Basin in northern New Mexico. This is one of the few known successions of fossiliferous red-bed siliciclastic sediments encompassing the Pennsylvanian-Permian boundary in the American Southwest and thus may inform questions regarding changing paleoclimate in tropical Pangea across the Pennsylvanian-Permian boundary. The section consists mainly of silty mudstones and sandstones with sheet-like to ribbon geometry and very minor limestones and records an upward transition from mainly braided stream deposition in the El Cobre Canyon Formation to anastomosing stream deposition in the Arroyo del Agua Formation.

We recognized multiple paleosol types within these strata, including calcic Protosols, calcic Argillisols, argillic Calcisols and Calcisols, all generally consistent with the interpretation of a seasonal sub-humid to semi-arid climate. The calcretes in these paleosols occur primarily as truncated profiles. Although Calcisols occur in both formations, we note that Protosols are more common in the El Cobre Canyon Formation, and Argillisols dominate in the Arroyo del Agua Formation. Also, we find that the calcretes in the Arroyo del Agua Formation are generally thicker than those in the underlying El Cobre Canyon Formation. The difference in calcrete maturity could be explained by changes in source-area relief and sedimentation rate. However, stable isotope analyses of pedogenic carbonate indicate that a significant enrichment of $\delta^{18}O$ occurs near the transition between the two formations, which approximates the Virgilian-Wolfcampian (equals Gzhelian-Asselian) boundary. Although the $\delta^{13}C$ data suggest that pCO_2 remained stable during the interval of deposition, the $\delta^{18}O$ data are consistent with the interpretation of climate aridification across the Pennsylvanian-Permian transition, potentially related to the onset of Gondwanan glaciation in the earliest Permian.

© 2018 Elsevier B.V. All rights reserved.

1. Introduction

The uppermost Carboniferous through lower Permian strata of tropical Pangea are widely recognized as containing valuable paleoclimatic archives that have the potential to increase our understanding of the timing and mechanisms of late Paleozoic global change. In particular, major questions remain regarding environmental changes coincident with the closing stages of Gondwanan glaciation and its relationship to increasing atmospheric pCO_2, the northward migration of Pangea, orogenic uplifts in central Pangea, potential changes in patterns of atmospheric circulation and the interpreted aridification of the Pangean interior during the late Paleozoic (e.g. Parrish, 1993; Dinterman et al., 2000; Kessler et al., 2001; Soreghan et al., 2002; Tabor and Montañez, 2002, 2004; Mack et al., 2003; DiMichele et al., 2006; Mountney, 2006; Montañez et al., 2007, 2016; Tabor et al., 2008; Giles et al., 2013; Montañez and Poulsen, 2013; Zhu and Tabor, 2014; Tanner and Lucas, 2017). Multiple studies have suggested that the moist subhumid-climate (*sensu* Cecil, 2003) that prevailed at tropical latitudes in Pangea during the latest Carboniferous (Virgilian) was replaced during the earliest Permian (Wolfcampian) by arid conditions that became widespread across central Pangea and as far north as the (subtropical) Appalachian basin (Tabor and Montañez, 2002, 2004; DiMichele et al., 2006; Tabor et al., 2008; Cecil, 2013). This change is attributed by some to reorganization of atmospheric circulation by the initiation of the Pangean megamonsoon during the Pennsylvanian, marking the end of a stable zonal system of atmospheric circulation, or to climate

* Corresponding author.
E-mail addresses: TannerLH@Lemoyne.edu (L.H. Tanner), Spencer.Lucas@state.nm.us (S.G. Lucas).

https://doi.org/10.1016/j.sedgeo.2018.05.014
0037-0738/© 2018 Elsevier B.V. All rights reserved.

change at the end of late Paleozoic Gondwanan glaciation (Kutzbach and Gallimore, 1989; Parrish, 1993; Kutzbach and Ziegler, 1993; Gibbs et al., 2002; Peyser and Poulsen, 2008; Tabor and Poulsen, 2008).

However, the specific mechanisms responsible for this apparent climate shift are not well understood as yet because, as stated by Tabor and Poulsen (2008), although there are useful and well-resolved records for climate change across the Carboniferous-Permian boundary, they generally are not well constrained temporally. Indeed, the timing of the onset of aridification, its extent, and correlation with trends in sea-level change and Gondwanan glaciation are all poorly resolved questions and topics of serious investigation. For example, Tabor et al. (2008) suggested, on the basis of paleosol morphologies, that different regions of equatorial Pangea experienced changing precipitation trends at differing times. Specifically, they suggested that some areas experienced a gradual trend of drying through the Virgilian, continuing into the Wolfcampian, other areas dried in the early Wolfcampian (Asselian to Sakmarian), and still other regions did not become arid until Leonardian time (Tabor et al., 2008, Fig. 4). Conversely, Schneider et al. (2006), in examining the trend of Permian aridification in the northern Tethyan region, noted a humid pulse during the earliest Wolfcampian (early Asselian), a time during which drying is documented in western equatorial Pangea (Tabor and Montañez, 2002, 2004; Tabor et al., 2008). Relevant to understanding the environmental complexities of this time interval are recent efforts to establish the potential coupling of climate, paleo-pCO_2, Gondwanan glaciation and sea level (Cecil et al., 2003; Montañez et al., 2007, 2016; Peyser and Poulsen, 2008).

The sedimentology of formations deposited during the interval spanning the Carboniferous-Permian boundary, and the paleopedology in particular, have provided valuable clues for addressing the questions of paleoenvironmental change described above. Indeed, many authors have described specific paleosol morphologies, clay mineralogy or the stable isotopic composition of pedogenic minerals in support of the interpreted paleoclimate transition (e.g. Kessler et al., 2001; Tabor and Montañez, 2002, 2004; Mack et al., 2003; DiMichele et al., 2006; Montañez et al., 2007; Tabor et al., 2008; Giles et al., 2013; Zhu and Tabor, 2014; Mujal et al., 2018). However, continuous stratigraphic sections with well-exposed paleosols that extend through the temporal interval of presumed climate shift are few. Hence, many of the aforementioned studies present pedogenic evidence from this time interval in only broad, regional terms, rather than describing the vertical trends from specific stratigraphic sections and presenting the relevant paleosol profiles; paleopedogenic evidence is thus presented as snapshots comparing pedogenic features of different ages from differing locations. Here, we attempt to add resolution to our understanding of the nature and timing of paleoclimate change during this transitional interval by presenting in detail the paleopedologic features and supporting isotopic data from a single, continuous stratigraphic section of the Upper Pennsylvanian (Virgilian) to lower Permian (Wolfcampian) Cutler Group in northern New Mexico.

2. Background

2.1. Location

The section studied here is located in Cañon del Cobre (El Cobre Canyon), a large north to north-east trending box canyon in southeastern Rio Arriba County, New Mexico, along the southeastern border of the Colorado Plateau (Fig. 1). Strata of Pennsylvanian, Permian, Triassic and Cenozoic age are exposed on the canyon floor, walls and rim (Smith et al., 1961; Fracasso, 1987; Kempter et al., 2007; Lucas et al., 2010a). The oldest strata exposed in the canyon are siliciclastic red beds of the El Cobre Canyon Formation of the Cutler Group, of Late Pennsylvanian-early Permian (Virgilian-Wolfcampian) age. The exposed El Cobre Canyon Formation strata are about 230 m thick (total thickness ca. 640 m) and are mostly siltstone and sandstone that rest on Proterozoic granitic basement. The overlying lower Permian Arroyo del Agua Formation of the Cutler Group is as much as 160 m thick, and also consists mostly of siltstone and sandstone. An extensive unconformity separates Cutler Group strata from overlying Late Triassic strata of the Shinarump Formation (Chinle Group) around the rim of Cañon del Cobre (Fig. 2).

2.2. Age

Paleobotanical collections from the El Cobre Canyon Formation strata are composed of taxa typical of the Late Pennsylvanian, including the genera *Alethopteris*, *Macroneuropteris*, *Sphenophyllum* and *Calamites*, a typical floral assemblage for a wetland-floodplain environment described initially as representative of the Virgilian (DiMichele and Chaney, 2005; DiMichele et al., 2010). Palynomorphs from the same

Fig. 1. Location of the measured section in north-central New Mexico. The base of the measured section is at 36° 17.228′N, 106° 20.641′W. Inset map (modified from Tanner and Lucas, 2017) illustrates major paleogeographic features, including uplifts of the Ancestral Rocky Mountains.

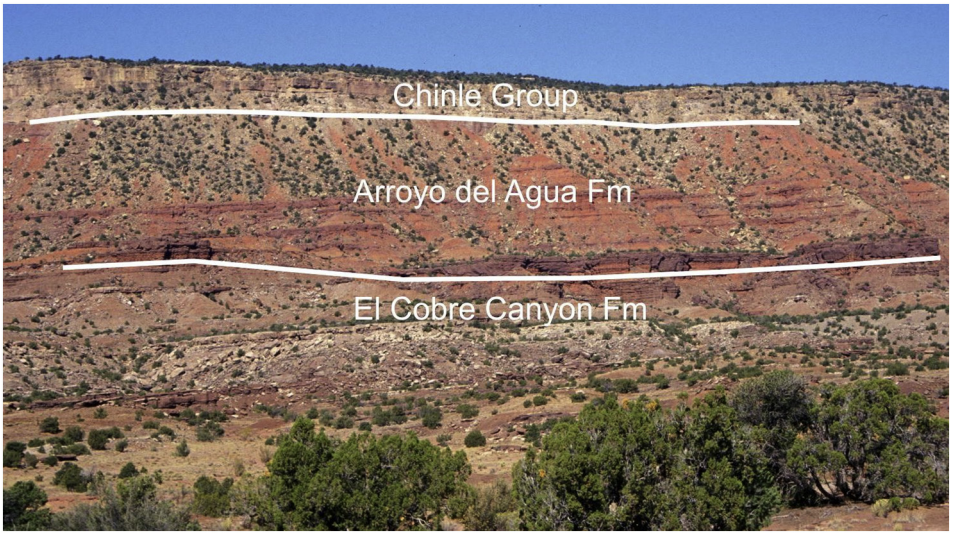

Fig. 2. Overview of the outcrop exposure on the western wall of Cañon del Cobre. The canyon is floored by the El Cobre Canyon Formation, overlain by the Arroyo del Agua Formation, which is truncated by the Upper Triassic Chinle Group (Shinarump Formation).

strata are broadly assigned to the Late Pennsylvanian (Utting and Lucas, 2010).

The Arroyo del Agua Formation is unproductive for floral remains. Tetrapod taxa from the El Cobre Canyon Formation at Cañon del Cobre that are characteristic of the Late Pennsylvanian include the diadectomorphs *Desmatodon*, *Limnoscelis* and *Diasparactus* (Lucas et al., 2010b), the eupelycosaur *Ophiacodon navajovicus* and the temnospondyl *Eryops*. The eupelycosaur *Edaphosaurus novomexicanus* is found in the same assemblage, and Lucas et al. (2010b) consider it more primitive in form than typical early Permian representatives, and thus, more likely Pennsylvanian than Permian in age. The eupelycosaur *Sphenacodon ferox* spans the uppermost El Cobre Canyon Formation to the upper Arroyo del Agua Formation, and the diadectomorph *Diadectes* occurs only in the upper Arroyo del Agua Formation. Hence, Lucas et al. (2010b, 2015), see also Lucas, 2018 placed the Virgilian-Wolfcampian boundary broadly within the uppermost El Cobre Canyon Formation (Figs. 3-4).

2.3. Previous work

The sedimentology of the Cutler Group at and near Cañon del Cobre has been studied previously. Eberth and Miall (1991) studied the sedimentology of the Cutler Group strata in considerable detail and found that deposition was controlled by southerly to southwest-flowing streams sourced from the Uncompahgre uplift just to the north of the study area (Fig. 1). Eberth and Miall (1991) divided Cutler strata, at that time designated the Cutler Formation, into three megasequences that define fundamental changes in sedimentological processes during deposition of the formation. Megasequence 1 was defined by broad, sheet-like sandstone bodies deposited by shallow braided channels, with thinner sandy to silty sheets interbedded within the intervening mudstones, recording frequent flooding of the inter-channel areas, forming sandy splays and floodplain ponds. The succeeding megasequence 2 is distinguished from megasequence 1 by a change in depositional style that is characterized by narrower, ribbon-like sandstones interpreted as channel deposits stabilized within the broad surrounding floodplains (anastomosing channels) with mature calcretes developed in the floodplain paleosols. The very top of the succession, not exposed in Cañon El Cobre, is characterized by a return to coarser sedimentation, interpreted as the result of renewed source-area uplift, marking the initiation of megasequence 3. Significantly, Eberth and Miall (1991) noted the occurrence of more calcrete in megasequence 2 than in megasequence 1, accompanied by a decrease in invertebrate trace fossils, both of which they considered evidence for a trend of increasing aridity during deposition of the two megasequences.

Lucas and Krainer (2005a, 2005b) defined the El Cobre Canyon and Arroyo del Agua formations, corresponding approximately to megasequence 1 and 2 of Eberth and Miall (1991), respectively, comprising the Cutler Group in the Chama Basin. They noted also a change in the color of the mudstones at the stratigraphic level where they placed the boundary between the formations. Krainer and Lucas (2010), in a detailed sedimentologic and petrologic study, reexamined the Cañon del Cobre section. Their lithostratigraphic description of the section (Fig. 4) matches well with that of Eberth and Miall (1991), and they generally agree with the sedimentologic, paleogeographic and

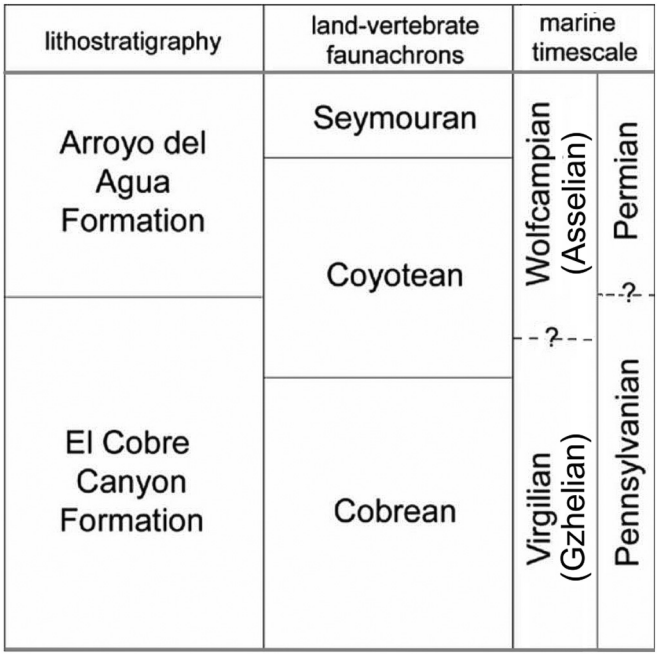

Fig. 3. Lithostratigraphic-biostratigraphic correlation of the Cutler Group formations (adapted from Lucas et al., 2010b) with both North American stage names and international (ICS) terminology (in parentheses; Gradstein et al., 2012).

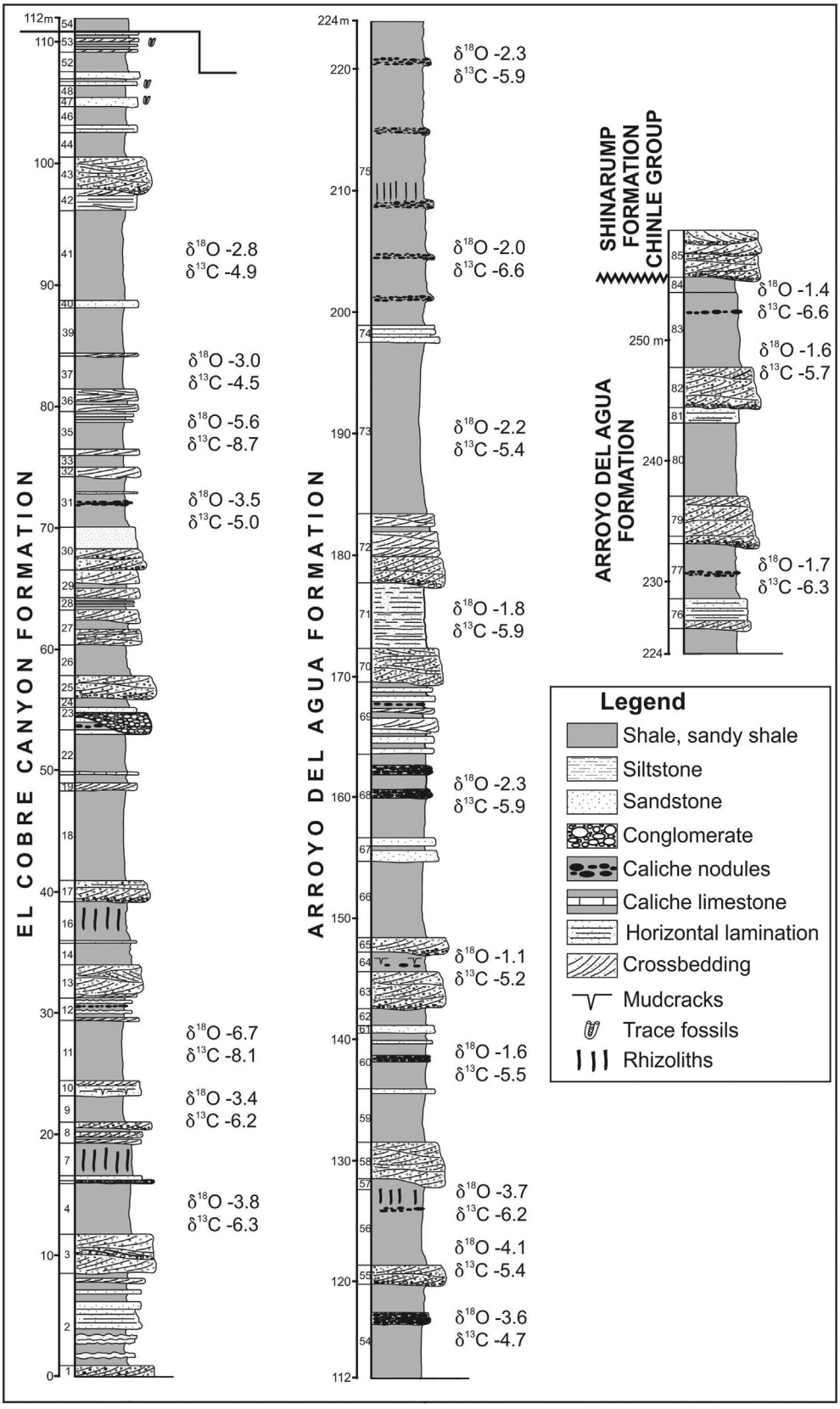

Fig. 4. Cutler Group section measured in Cañon del Cobre (adapted from Krainer and Lucas, 2010), with approximate boundary between El Cobre Canyon and Arroyo del Agua formations. Numbers within column designate measured lithologic units referred to in text. Positions of carbonate samples analyzed for isotopic data (Table 1) shown.

paleoclimatic interpretations of the earlier authors. Thus, the Cañon de Cobre, megasequence 1 of Eberth and Miall encompasses the El Cobre Canyon Formation, whereas their megasequence 2 is most of the Arroyo del Agua Formation. The boundary between the megasequences is in the lower part of the Arroyo del Agua Formation, rather than at the formational boundary (Krainer and Lucas, 2010).

Table 1
Isotopic analyses of Cutler Group carbonates.

Sample ID	Stratigraphic unit #	$\delta^{13}C$ ‰ PDB	$\delta^{18}O$ ‰ PDB
EC-1	4	−6.3	−3.8
EC-2	9	−6.2	−3.4
EC-3	11	−8.1	−6.7
EC-4[a]	31	−5.0	−3.5
EC-5	35	−8.7	−5.6
EC-6	37	−4.5	−3.0
EC-7	41	−4.9	−2.8
EC-8	54	−4.7	−3.6
EC-9	56	−5.4	−4.1
EC-10	56	−6.2	−3.7
EC-11	60	−5.5	−1.6
EC-12	64	−5.2	−1.1
EC-13	68	−5.9	−2.3
EC-14[a]	71	−5.9	−1.8
EC-15	73	−5.4	−2.2
EC-16	75	−6.6	−2.0
EC-17	75	−5.9	−2.3
EC-18	77	−6.3	−1.7
EC-19	83	−5.7	−1.6
EC-20	83	−6.6	−1.4

[a] Potential palustrine carbonate.

3. Methods

For this study, the Cutler Group in Cañon del Cobre was reexamined with the specific goal of describing the pedogenic features, using the context of the previously published lithostratigraphic framework. In addition to field measurements and descriptions of these features, carbonate samples were collected for petrographic examination and stable isotope analysis. Petrographic studies were conducted on standard petrographic thin sections of 30 μm thickness. Carbonate samples were collected for isotopic analysis by selectively drilling micritic calcite in lapped slabs corresponding to prepared thin sections with an ultrafine engraving tool while viewing under a binocular microscope.

The samples were analyzed for $\delta^{13}C$ and $\delta^{18}O$ by the Duke Environmental Stable Isotope Laboratory (Nicholas School of the Environment, Duke University, Durham, North Carolina), by reacting the carbonate for one hour with 100% H_3PO_4 at 72 °C using a ThermoFinnigan (Bremen) GasBench II with CombiPAL autosampler and equilibration modules. Sample gases from the GasBench were analyzed by continuous flow with a ThermoFinnigan Delta+XL IRMS. Raw isotope data were normalized using NBS-19, IAEA CO-8, and an internal reference (Merck calcium carbonate). Precision is approximately 0.1 per mil at 1 sd for both $\delta^{13}C$ and $\delta^{18}O$. Results are reported in Table 1 in parts per thousand (‰) relative to the Pee Dee Belemnite standard (PDB). The mineralogy of the carbonate and of the clay mineral assemblage were determined by X-ray diffraction analysis of bulk powder samples and clay separates with a Bruker Phaser D2 X-ray diffractometer using a Cu-anode tube operating at 30 kV and 10 mA. All carbonate was determined to be low-Mg calcite, and the clay mineral assemblage is dominated by illite-chlorite, with no significant changes in composition or proportion through the section.

4. Pedogenic features

4.1. El Cobre Canyon Formation paleosols

Those paleosols in the section that display sufficiently distinctive horizonation to permit classification are described herein using the terminology of Mack et al. (1993). We assign names to paleosol orders, with modifying adjectives that describe the most prominent secondary characteristic. The strata of the El Cobre Canyon Formation contain a wide range of paleosol types formed on the floodplain deposits, from Protosols to Calcisols, with the units we interpret as Protosols and calcic Protosols most common. The occurrences and characteristics of these paleosols are described below.

4.1.1. Protosols

The lower El Cobre Canyon Formation contains multiple intervals of slope-forming mudstone, particularly in the lower part of the formation. Weathered mudstone slopes are typically veneered by loose, cm-scale calcareous nodules and rhizoliths (Fig. 5A). Where visible, the most common mudstone fabrics vary from blocky to crumb fabric, although visible cutans are generally lacking (Retallack, 2001). Several of these meter-scale mudstone units display very slight changes in the color of the mudstone, reddening and darkening slightly downward, from 10YR 7/6 downward to 2.5YR 4/4. We regard this as evidence of incipient horizonation, i.e., there is no clear distinction between A and B horizons, but separation had begun by eluviation of the upper soil and illuviation below, as in modern Entisols (Schaetzl and Thompson, 2015). We term these units Protosols, or calcic Protosols where they contain calcareous nodules (Fig. 5B). The calcretes in the calcic Protosols are immature, mainly Stage II (*sensu* Gile et al., 1966; Machette, 1985) in which individual nodules are discrete and separated from adjacent nodules. Calcareous nodules are common in most mudstone beds in the section, regardless of visible evidence of horizonation. These vary from small (1 to 5 cm) bodies with diffuse boundaries that are exposed as a nodular weathering fabric to nodules with well-defined boundaries and less commonly isolated botryoidal masses 10 cm to 20 cm in diameter.

4.1.2. Calcisols

Mature calcrete beds (Stage III to IV *sensu* Gile et al., 1966; Machette, 1985), with coalescing nodules that form laterally continuous (Bk) horizons are less common than Stage II calcretes, but they do occur at multiple levels throughout the section. A pedogenic origin for these features is indisputable given the common association of roots and

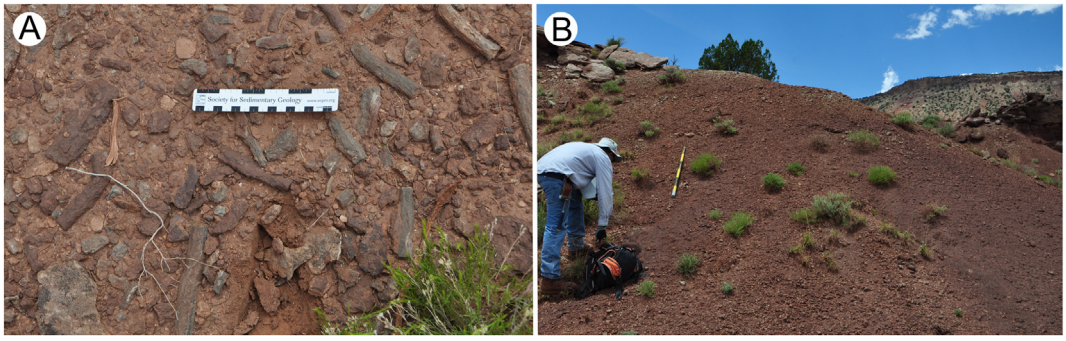

Fig. 5. Pedogenic features of the El Cobre Canyon Formation. A) Weathered mudstone slope covered by elongated rhizoliths and irregular carbonate clasts presumed to be of eroded clasts of calcrete. B) Calcic Protosol in unit 11 displays very subtle color change, darkening from upper part, above the 1.5 m staff, to the lower portion. Ped structure is granular to crudely blocky. B) Marly limestone bed with sharp base and prominent drab root traces in unit 18. Hammer is 26 cm long.

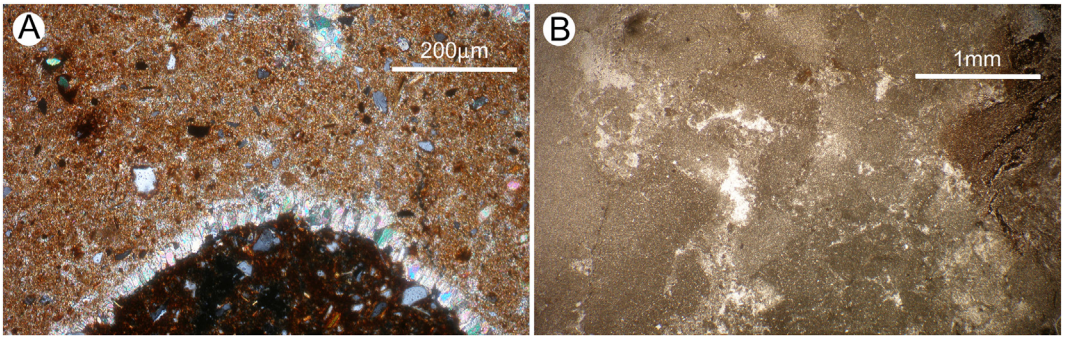

Fig. 6. Microscopic views of fabrics in the carbonates of the Cutler Group. A) View of alpha fabric in calcrete nodule (unit 56, Fig. 4; lower Arroyo del Agua Formation) illustrating bladed calcite corona coating mudstone clasts (nicols crossed). B) Micrite with clotted peloidal/brecciated fabric typical of beds interpreted as palustrine carbonates (unit 35, Fig. 4; El Cobre Canyon Formation, nicols uncrossed).

calcareous nodules in these strata. Moreover, petrography reveals the presence of typical alpha-type calcrete fabrics in the nodules, such as grain coronas and corroded floating grains that indicate that these nodules represent the accumulation of carbonate in the B horizon of paleosols (Fig. 6A; Alonso-Zarza and Wright, 2010a). Thus, we are confident in our interpretation that these carbonates represent calcretes formed within soils developed on alluvial muds.

The mudstone-hosted calcareous nodule horizons represent simple Stage II to III calcrete profiles (Gile et al., 1966; Esteban and Klappa, 1983; Machette, 1985). Mature (Stage III to IV) calcretes typically have upper surfaces that vary from transitional with overlying mudstone to, more commonly, abruptly truncated (sharp) surfaces. The bases of the nodular horizons are typically gradational, transitioning downward to discrete, vertically-stacked cm-scale nodules (rhizocretions) and isolated nodules. In profiles where calcareous B horizons (Btk if argillic and calcic, as in Stage II calcrete, or Bk for Stage III calcrete) are more prominent than the argillic (Bt) horizons, we assign the designation argillic Calcisol or Calcisol, as appropriate. Many of the paleosols in the section are compound paleosols (*sensu* Kraus, 1999) that display multiple B horizons. The compound profiles we recognize in the section are marked by the repetition of specific types of B horizons (Bt, Btk or Bk) without an intervening A horizon, suggesting interruption of sedimentation and an intervening erosional episode. This pattern is noted in mainly some argillic Calcisol and Calcisol profiles. Presumably this reflects the erosional resistance of the calcrete during floodplain erosion, likely during channel migration.

Mature calcretes occur in unit 4 of the El Cobre Canyon Formation, near the base of the measured section in a compound Calcisol (Figs. 4, 7A). At the best exposure of this unit, the profile is 1.4 m thick and contains up to four nodular (Bk) horizons. Individual nodular horizons are up to 40 cm thick and most display evidence of erosional truncation (Fig. 7B, D). The nodular horizons, particularly the upper- and lowermost, consist of coalesced masses of calcareous nodules at the top, with the density and size of individual nodules decreasing downward. However, the upper portions of these horizons, although consisting of coalesced calcareous nodules, lack the platy fabric or horizontal lamination characteristic of Stage IV calcretes. Therefore, we describe these as Stage III calcretes. The nodular horizons locally impart a discoidal to

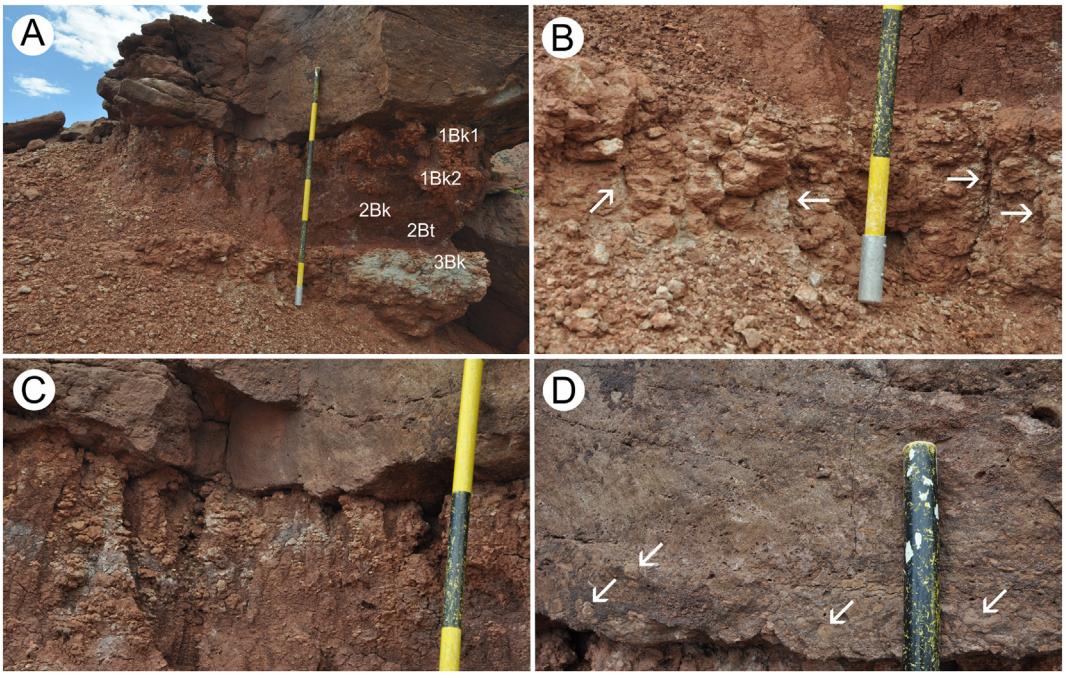

Fig. 7. Compound Calcisol (unit 4, Fig. 2) in El Cobre Canyon Formation. A) Overview of the compound profile with multiple Bk horizons. The two uppermost Bk horizons show evidence of an intervening erosional episode. Divisions on staff are 0.25 m. B) Detail of horizon 3Bk illustrating crude platy-prismatic fabric and penetration by root traces (arrows). C) Detail of 1Bk1 horizon in A) illustrating erosional truncation and prismatic fabric. D) Basal channel-fill that truncates 1Bk1 is an intraformational conglomerate consisting of erosional reworked calcrete clasts (arrows).

prismatic fabric to the paleosol (Fig. 7B - D; Retallack, 2001). Drab root traces occur in association with these horizons (Fig. 7B). These are drab (bluish-gray, 5BG 8/1 to 10BG 8/1) traces that stand out by their color contrast from the surrounding reddish-brown (2.5YR 7/4 to 2.5YR 5/4) mudstone and are up to 40 cm in vertical length. The uppermost Bk horizon is truncated by an overlying channel-fill deposit that consists at its base of intraformational conglomerate comprising mainly reworked calcrete nodules (Fig. 7D).

We note that the quality of the exposure of this particular profile is very localized; laterally, the quality of the exposure declines abruptly, perhaps explaining the failure of previous studies to note the presence of mature calcretes this low in the stratigraphic section at this location (Eberth and Miall, 1991; Krainer and Lucas, 2010). Another mature calcrete, a simple Calcisol occurs at the top of unit 41 (Fig. 4). The single Bk horizon is 0.8 m thick and displays features similar to those of the nodular horizons in unit 4; the nodules are coalesced at the top of the horizon, which has a semi-prismatic fabric, and nodule size and density decreases downward at the base. We regard this calcrete also as having a maturity of Stage III.

4.1.3. Palustrine limestones

Several of the slope-forming mudstone units are interrupted by calcareous ledges with nodular upper contacts and sharp lower contacts, as in units 18, 25 and 31 (Figs. 4, 8A, B). These ledges range in thickness from 10 cm to 40 cm, have limited lateral extent, are mottled gray-brown to pink in color, and, where well-exposed, display brecciated fabrics and prominent drab greenish-gray vertical root traces that commonly penetrate the entire thickness of the ledge. Eberth and Miall (1991) noted the presence of several of these decimeter-scale beds of muddy limestone, which they described as “flat-based marl.” Eberth and Miall (1991) interpreted these as floodplain pond deposits, rather than pedogenic carbonates. We agree with this interpretation with the addendum that we regard these as floodplain pond or wetland deposits that have undergone some degree of desiccation and pedogenic modification, i.e., palustrine carbonates (*sensu* Alonso-Zarza, 2003; Alonso-Zarza and Wright, 2010a) based on the geometry, nature of the upper and lower contacts, penetration by roots and the brecciated fabric.

In thin section, these beds display brecciated and peloidal fabrics with circumgranular cracks, all commonly regarded as features of palustrine sediments (Fig. 6B) (Plaziat and Freytet, 1978; Platt, 1989, 1992; Platt and Wright, 1992; Armenteros et al., 1997; Tanner, 2000; Freytet and Verrecchia, 2002; Alonso-Zarza, 2003; Alonso-Zarza and Wright, 2010a). These fabrics formed by desiccation and root penetration of the original sediments, resulting from shrinkage cracking during periods of emergence, typically under sub-humid to semiarid conditions (Platt and Wright, 1992; Armenteros et al., 1997). Some beds exhibit nearly vertical fissures that were likely created by solution enlargement of root channels, suggesting prolonged subaerial exposure (Fig. 8B; Platt, 1989). This brecciated limestone facies is interbedded vertically and laterally gradational with the mudstone facies described above, so it likely represents deposition in shallow lakes and ponds that occupied topographic lows on a broad floodplain and were mainly ephemeral.

4.2. Arroyo del Agua Formation

The Arroyo del Agua Formation contains a higher proportion of mudstone than the underlying El Cobre Canyon Formation (Fig. 4), and most of the mudstone units display obvious indications of pedogenesis. The flat-based marl/limestones in the El Cobre Canyon Formation that we interpret as palustrine deposits occur also in the Arroyo del Agua section, but are less common.

4.2.1. Argillisols

Paleosol profiles with a discernible eluviated upper (A) horizon in the section (i.e., complete profiles) are absent in the El Cobre Canyon Formation but do occur in the Arroyo del Agua Formation (Fig. 9A); they are less common than truncated profiles, however. Those profiles clearly displaying distinct A and B horizons are mainly Argillisols and calcic Argillisols, denoting a paleosol in which the B horizon contains illuviated clay (Retallack, 2001; Schaetzl and Thompson, 2015). The A horizons are lighter in color than the B horizons, suggesting eluviation, and generally reddish yellow (7.5YR 7/6). The most common paleosol type we find in the Arroyo del Agua Formation is the calcic Argillisol, denoting a paleosol displaying a prominent horizon in which the primary characteristic is a clay-rich B horizon that is distinctly enriched in $CaCO_3$ in the form of nodules (Stage II calcrete), but the nodules are not the primary characteristic, i.e., a Btk horizon (Retallack, 2001; Schaetzl and Thompson, 2015). The greater thickness of this formation is occupied by Argillisols and calcic Argillisols.

In some units, stacked profiles with multiple A, Bw, Bt or Btk horizons are distinguishable, as seen near the formation base (unit 54) and higher up (unit 73, Figs. 4, 9A). The A horizon in these profiles is lighter in color, typically yellowish-brown (10YR 6/4), than the darker reddish-brown (2.5YR 5/4) B horizon. Mudstone fabrics vary from crumb to blocky, with very weakly developed cutans. We designate as calcic Argillisols those profiles where the B horizon contains isolated concentrations of nodular-weathering carbonate, although the nodule boundaries may be diffuse. One such occurrence of a Btk horizon (lower unit 75; Fig. 4) is distinctive for the presence of prominent sand-filled root casts, up to 10 cm in diameter and 50 cm in length (Fig. 9B). Another distinctive Btk horizon occurs in unit 66 where funnel-shaped vertical cylinders are up to 5 cm in diameter and 25 long and display a subhorizontal parting that imparts a ‘poker-chip’ structure to the casts (Fig. 9C) that some authors (e.g., Dubiel et al., 1987) have attributed to the aestivation burrows made by lungfish. Other authors (e.g., Tanner and Lucas, 2007), however, have pointed out that these criteria are not diagnostic and that root casts of large

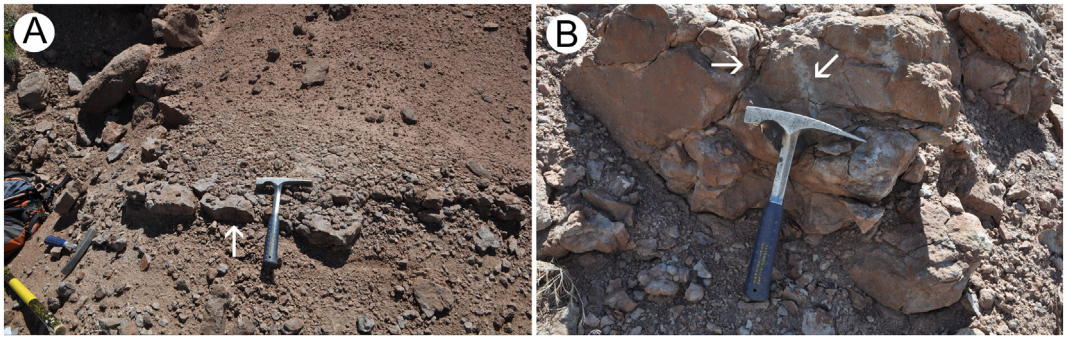

Fig. 8. Flat-based marl in El Cobre Canyon Formation. A) Overview of the bed (unit 22, El Cobre Canyon Formation). Upper contact has a weathered, nodular surface. Basal contact is abrupt with the underlying mudstone. B) Detail of the bed in A) illustrating drab root traces (right arrow) and solution enlarged root channel (left arrow). Hammer (for scale) is 26 cm long.

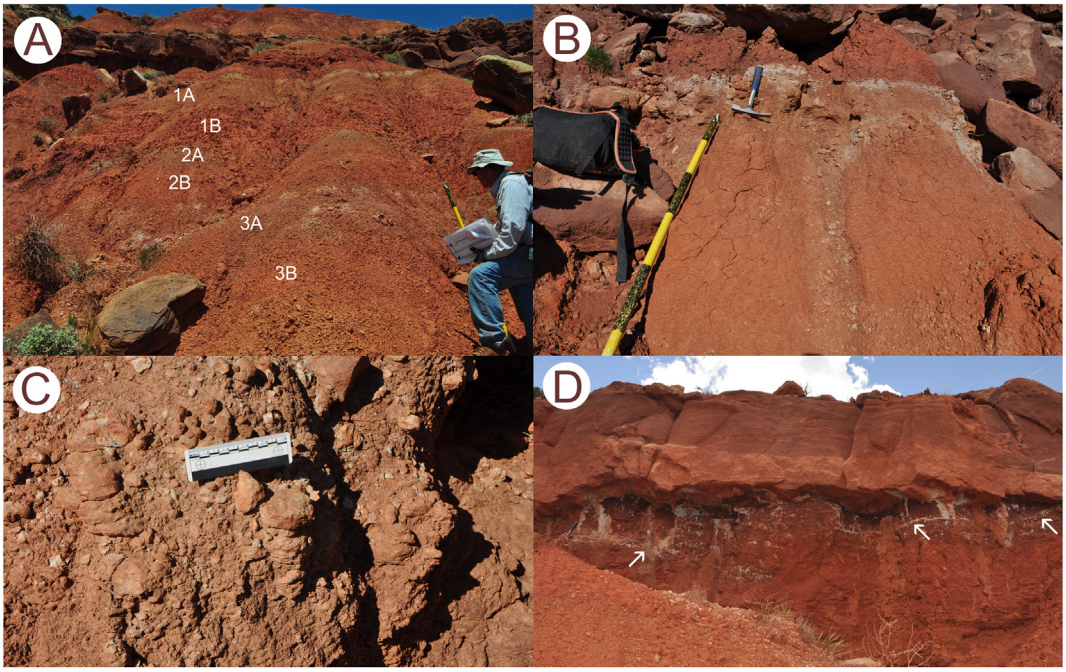

Fig. 9. Pedogenic features of Arroyo del Agua Formation. A) Multiple profiles of Argillisols in unit 73, Fig. 4) distinguished by repeated A-B horizons. B horizons characterized by a blocky ped fabric. B) Large-diameter cast of a monopodial root system (to the right of hammer), in lower part of Unit 75 (Fig. 4), presumably filled by sand originally, now excavated by erosion. C) Downward-tapering, funnel-shaped rhizoliths in unit 66 (Fig. 4). D) Mudstone at top of unit 75 (Fig. 4) is penetrated by sandstone-filled desiccation cracks and contains arcuate, subhorizontal vertic fractures (arrows).

monopodial vegetation can produce similar features. We follow the latter interpretation in this instance.

4.2.2. Vertisols

The top of unit 75 is unique for the occurrence immediately below a channel-fill sandstone ledge of subhorizontal vertic fractures, highlighted by reduction banding, that extend up to 1 m in length (Figs. 4, 9D). We regard this mudstone as a truncated Vertisol.

4.2.3. Calcisols

Calcisols and argillic Calcisols were found at only three levels in the formation. The top of unit 64 displays a truncated compound Calcisol containing multiple Bk horizons (Figs. 4, 10A, B). The uppermost nodule horizon (0.2 m thick), which is overlain directly by channel-fill sandstone, merges laterally with another thin nodule layer that slopes downward, possibly following a scour surface. The underlying Bt horizon separates the thin Bk horizons above from the thick (0.8 m),

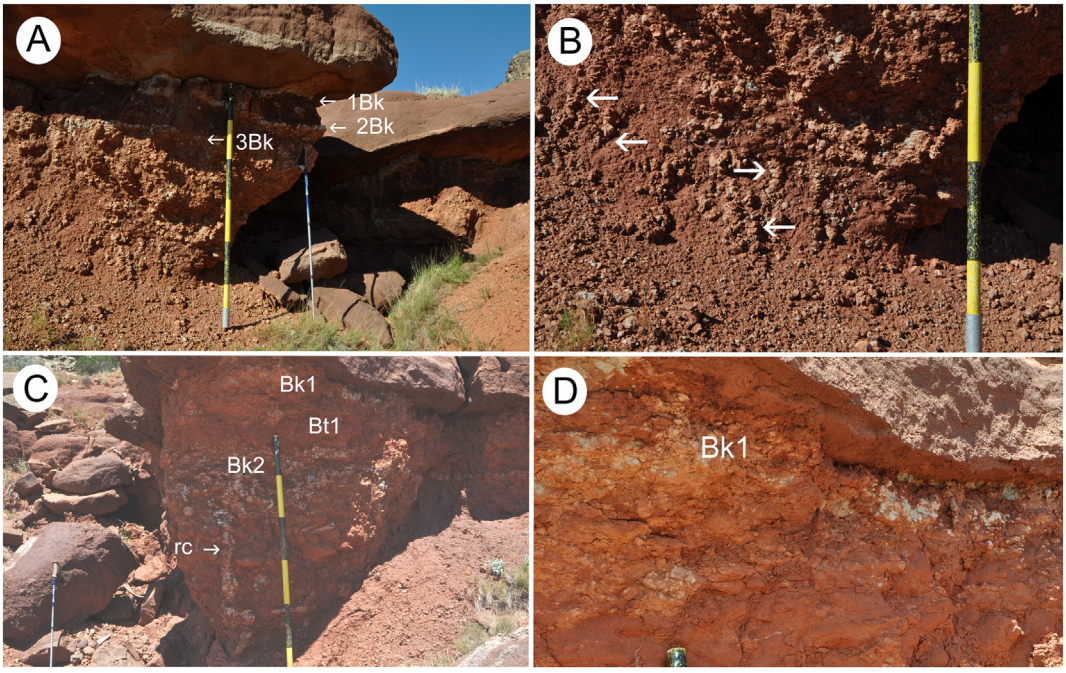

Fig. 10. Calcisols of the Arroyo del Agua Formation. A) Compound Calcisol profile at the top of unit 64 (Fig. 4) displays multiple truncated Bk horizons. B) The base of the 3Bk horizon (in A) contains rhizocretions (arrows) consisting of vertically stacked carbonate nodules. C) Composite argillic Calcisol (unit 75, Fig. 4) in which the two Bk horizons are separated by a Bt horizon. An extended rhizocretion (rc) extends downward from the base of Bk2. D) Detail of Bk1, which is sharply truncated by the overlying channel-fill sandstone.

truncated Bk horizon below. The lower portion of this horizon is dominated by vertically stacked nodules (rhizocretions). A well-developed composite argillic Calcisol occurs in the lower part of unit 75 (Figs. 4, 10C, D). The top of the profile is a 0.3 m-thick Bk horizon with Stage III calcrete, i.e., coalesced nodules that decrease in abundance downward in the underlying mudstone. Unlike the compound profiles described above, there is no evidence of erosional truncation of the lower Bk horizon, which is up to 0.4 m thick. Very distinctive rhizocretions extend up to 0.8 m below the base of this horizon.

4.2.4. Summary of Cutler Group paleosols

In summary, the El Cobre Canyon strata are dominated by Protosols and calcic Protosols, with subordinate Calcisols, whereas Arroyo del Agua Formation paleosols are dominantly Argillisols and calcic Argillisols. Argillic Calcisols and Calcisols also occur in the Arroyo del Agua Formation and are more common than in the underlying El Cobre Canyon Formation. Sand-filled desiccation cracks and arcuate fracture planes (vertic fractures) are prominent only near the top of the Arroyo del Agua Formation (top of unit 75, Figs. 4, 9D).

5. Geochemistry

Analysis by X-ray diffraction confirms that all of the carbonate beds sampled in this study consist of low-Mg calcite. A pedogenic origin for most bedded carbonate was indicated by field relationships, such as nodular fabrics and a gradational base, as well as by petrographic features, such as the presence of typical alpha-type calcrete fabrics in the nodules and of grain coronas and corroded floating grains, all of which indicate that these nodules represent the accumulation of carbonate in the B horizon of paleosols (Allen and Wright, 1989; Birkeland, 1999; Retallack, 2001, 2005; Alonso-Zarza and Wright, 2010b; Schaetzl and Thompson, 2015). Carbonate beds observed to have sharp lower contacts with the underlying mudstone and exhibiting brecciated micritic fabrics but lacking the alpha fabrics described above are considered most likely to have a palustrine origin (Alonso-Zarza et al., 1992; Alonso-Zarza and Wright, 2010a). Of the samples analyzed for this study, EC-4 (unit 31) and EC-14 (unit 71) likely represent palustrine carbonate—carbonate sediment deposited in floodplain ponds or wetlands subjected to pedogenic reworking. We consider that all other samples represent only pedogenic carbonate. In regard to the pedogenic carbonate samples, we note that because most sampled profiles display evidence of erosional truncation, the depth of carbonate accumulation below the original sediment surface is not well constrained. Hence, no attempt is made to calculate mean annual precipitation from the depth of carbonate accumulation.

Results of isotopic analyses are presented in Table 1 and Fig. 11. Values of $\delta^{13}C$ range from −8.4‰ to −4.5 ‰ PDB, with a mean $\delta^{13}C$ −5.9 ± 0.2‰. With the exception of two outlier values of $\delta^{13}C <$ −8.0 ‰ (Fig. 11; EC-3 and EC-5), however, the $\delta^{13}C$ data demonstrate substantial consistency across the sampled stratigraphic interval. Indeed, since evaporative enrichment is a common characteristic of lacustrine carbonate, the consistency of the isotopic composition and lack of covariation of $\delta^{13}C$ and $\delta^{18}O$ suggests that the sampled carbonate is primarily pedogenic in origin, rather than lacustrine (Talbot, 1990; Talbot and Kelts, 1990), supporting the field observations. As noted above, however, we interpret two samples (EC-4 and EC-14) as having a palustrine origin, although the isotopic composition of these samples falls well within the range of the remaining sample set. Therefore, we include them within the data set for the purposes of calculating the mean. For the 20 samples collected across the entire section, $\delta^{18}O$ ranges from −6.7 to −1.1‰ PDB (mean $\delta^{18}O = -2.9 \pm 0.3$‰). Unlike the consistency exhibited by the $\delta^{13}C$ data, however, a clear trend is seen in the stratigraphic trend for the $\delta^{18}O$ data (Fig. 4, Table 1). Of greatest significance is the enrichment in $\delta^{18}O$ that occurs in the pedogenic carbonates of the Arroyo del Agua Formation, relative to those of the underlying El Cobre Canyon Formation, from a mean $\delta^{18}O$ of −4.0‰ PDB in the older formation to −1.8‰ PDB in the younger.

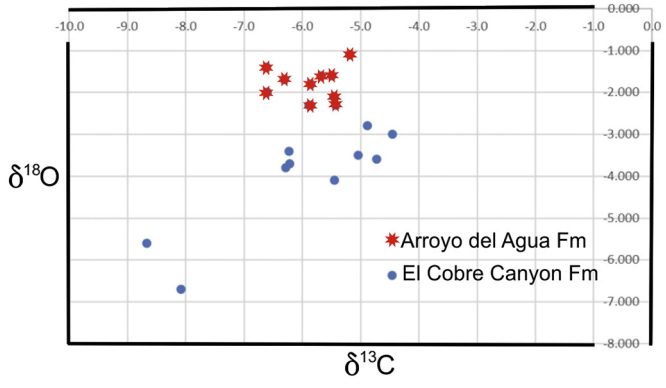

Fig. 11. Crossplot of $\delta^{18}O$ and $\delta^{13}C$ from the El Cobre Canyon and Arroyo del Agua formations illustrates the separation in oxygen isotope composition between the formations, but the near correspondence of the carbon isotope composition.

6. Discussion

6.1. Paleoclimatic interpretation of pedogenic features

In a general sense, the pedogenic features observed in both the El Cobre Canyon and Arroyo del Agua formations suggest overall seasonal, sub-humid shifting to potentially semi-arid paleoclimate conditions during the total span of time represented by their deposition. Pedogenic carbonate, the defining characteristic of most of the Cutler Group paleosols, accumulates during the dry season in regions that experience significant seasonal fluctuations in climate, but this encompasses a broad range of climates, from semi-arid to sub-humid (250 mm to >750 mm precipitation per year; Allen and Wright, 1989; Birkeland, 1999; Retallack, 2001, 2005; Alonso-Zarza and Wright, 2010b; Schaetzl and Thompson, 2015), or dry sub-humid to moist sub-humid (*sensu* Cecil, 2003). A seasonal distribution of precipitation also is required for the formation of vertic features in soils, which similarly form generally in semi-arid to sub-humid environments (500 mm to 1000 mm precipitation; Birkeland, 1999; Schaetzl and Thompson, 2015), but as noted above, these features are uncommon in the Cutler Group paleosols.

The differences in paleosol types between the El Cobre Canyon and Arroyo del Agua formations are subtle, but clear. Calcisols and/or argillic Calcisols occur in both formations, but we note that very weakly developed paleosols, Protosols and calcic Protosols, are much more common in the older El Cobre Canyon formation, and well-developed paleosols, Argillisols and calcic Argillisols, dominate in the younger Arroyo del Agua Formation. Moreover, calcrete (Bk) horizons are more abundant and thicker on average in the Arroyo del Agua Formation. Similarly, we observe fewer "flat-based marl" beds, or palustrine limestones in the younger formation. The differences between the El Cobre Canyon and Arroyo del Agua formations in pedogenic features and paleosol types are consistent with the interpretation of the onset of an increasingly dry climate near the Pennsylvanian-Permian (Virgilian-Wolfcampian equals Gzhelian-Asselian) boundary. As noted above, our analysis of the clay mineral assemblage shows no significant changes in mineralogy or proportions, suggesting that any climate change at this time was not sufficient to alter the mineralogy of weathering products during deposition of the Cutler Group.

The sedimentology of the Cañon del Cobre section is relevant to the interpretation of the conditions of paleosol formation. Eberth and Miall (1991) defined their megasequences 1 and 2, which correspond approximately to the later-defined El Cobre Canyon and Arroyo del Agua formations, based primarily on differences in fluvial style. Megasequence 1 contains laterally extensive sandstone sheets, interpreted

as the deposits of braided streams, whereas megasequence 2 sandstones display more of a ribbon geometry, interpreted as anastomosing stream deposits. Eberth and Miall (1991) interpreted the changes in grain size and fluvial style as recording a progressive decrease in source-area relief and sedimentation rate. This is worth noting because a decreased depositional gradient also could explain some of the pedogenic differences between the two formations. The lowering of the fluvial gradient, and thus lower stream energy, over time could decrease the rate of floodplain reworking and thereby allow the preservation of more complete (nontruncated) soil profiles with A and B horizons. Calcretes formed during deposition of the Arroyo del Agua Formation are generally thicker than those of the El Cobre Canyon Formation. This also may be a consequence, in part, of a decreased sedimentation rate due to the longer residence time of the B horizon in the soil-forming environment, allowing a longer period of accumulation of $CaCO_3$. Hence, although the differences in the pedogenic features between the El Cobre Canyon and Arroyo del Agua formations are consistent with gradual climate aridification, they are not by themselves definitive evidence of such a trend.

Shorter term (<1 Myr) variations in mean precipitation also are indicated by the intraformational variations in paleosol types. Whereas some variations in the maturity and thickness of calcretes can result from variations in the position on the floodplain, or catena, due to local variations in sedimentation rate, major changes over short stratigraphic intervals from Protosol or Argillisol to Calcisol are more likely due to fundamental variations in climate, such as precipitation and/or evaporation (Birkeland, 1999; Retallack, 2001; Mack et al., 2003; Schaetzl and Thompson, 2015). Therefore, we consider the evidence for greatly varying soil moisture demonstrated by the intraformational variations of paleosol types as significant. Calcrete can form under a rather wide variety of climatic conditions, but it is most commonly associated with at least seasonal soil moisture deficit at sub-humid to semi-arid conditions (Alonso-Zarza and Wright, 2010b). The stratigraphic proximity of Calcisols and Argillisols in the Cañon del Cobre succession suggests significant variations in soil moisture episodically. There is insufficient age constraint in the section we examined to determine the frequency of these variations. However, we note the published evidence for cyclical variation in pCO_2, and therefore, of climate, coinciding with periodic Gondwanan glaciation at the long eccentricity interval (ca. 405 kyr) through the end of the Pennsylvanian Period (e.g., Montañez et al., 2016). Notably, the latter part of the Pennsylvanian and early Permian periods represent time intervals during which portions of the Gondwanan landmass were experiencing episodic glaciation, ostensibly at the long eccentricity cycle frequency (ca. 405 kyr; e.g., Montañez et al., 2007, 2016). Hence, some amount of paleosol variability may be attributed plausibly to climate cyclicity with concomitant cyclical variations in precipitation as well as mean annual temperature.

6.2. Isotopic composition

The most significant result of the isotopic analyses of Cutler Group carbonates is the abrupt shift in $\delta^{18}O$ coinciding approximately with the boundary between the formations, which in turn is considered to approximate the Virgilian-Wolfcampian boundary. Fractionation during evaporation of soil moisture causes isotopic enrichment, but the level of enrichment varies by depth (Allison et al., 1984; Gat, 1996; Hsieh et al., 1998). More importantly, there are multiple causes for a change in the isotopic composition aside from climate change, including changes in latitude, tectonic uplift or orographic effects, and changed distance to the oceanic moisture source, accomplished via eustasy or changed prevailing wind direction (well-reviewed in Tabor and Poulsen, 2008). Some of these mechanisms, particularly those involving tectonic processes, would seem too gradual to explain the abrupt isotopic shift observed in the Cutler Group. Hence, we favor increased aridity as the more likely mechanism responsible for the $\delta^{18}O$ enrichment. This interpretation, of course, offers the advantage of being consistent with the pedogenic evidence presented herein. Notably, some of the mechanisms cited above may be linked, such as falling sea-level and local aridification due to increased distance from the source of atmospheric moisture, which we explore below.

Tabor and Montañez (2002) cited a mean value of $\delta^{18}O = -1.2‰$ (PDB) for soils formed in western equatorial Pangea during the Virgilian, enriched to $\delta^{18}O = +0.5‰$ (PDB) by the Wolfcampian, which the authors interpret as the result primarily of increased aridity. This is consistent with their observations of Virgilian paleosols comprising mainly Histosols, Ultisols and Inceptisols formed under humid nonseasonal conditions, and Alfisols, Entisols, Vertisols and vertic Calcisols formed under humid but seasonal conditions in the Wolfcampian. The isotopic shift exhibited here by the Cutler Group strata is of very similar magnitude, and thus accords well with this earlier report and interpretation.

Finally, we note the consistency of the $\delta^{13}C$ data across the sampled stratigraphic range in the Cutler Group, and the close agreement with the values obtained for the approximately correlative Sangre de Cristo Formation (Tanner and Lucas, 2017). Moreover, we note that our mean $\delta^{13}C$ of −5.9‰ matches well the values of ca. −6.0 reported for pedogenic carbonate from the Virgilian of the Pedrogosa Basin (southern New Mexico) and the early Wolfcampian (Asselian) of the Grand Canyon embayment (southern Colorado Plateau) (Montañez et al., 2007). As $\delta^{13}C$ is commonly used as a proxy for paleo-pCO_2 calculation (e.g., Ekart et al., 1999), the consistency of the Cutler Group data suggest stability of pCO_2 throughout the interval of deposition. Yet, an increase in pCO_2 across the Carboniferous-Permian has been cited by some authors (Tabor and Poulsen, 2008; Michel et al., 2015). The isotopic compositions of phyllosilicates and hematite formed in paleosols in north-central Texas (eastern shelf of the Midland Basin) were cited by Tabor et al. (2002, 2013a), Tabor and Montañez (2005) and Tabor (2007) as evidence of warming, the latter study interpreting an abrupt soil temperature warming of up to 13 °C across the system boundary.

The regional trends in floristic assemblages are complicated by apparent cyclical variations between wetter and drier assemblages (DiMichele et al., 2005; Tabor et al., 2013b); the timing of these cycles has been interpreted as glacially controlled. Superimposed on this cyclicity is an overall longer-term shifted from greater to decreased moisture and more pronounced seasonality spanning the Pennsylvanian-Permian boundary (Tabor et al., 2013b). In a more general sense, assemblages shifted from a cooler, wetter *Sigillaria* and pteridosperm-dominated biome in the Pennsylvanian, to a seasonally dry-adapted assemblage dominated by conifers, callipterids and other seed plants (DiMichele et al., 2009; Tabor et al., 2013a, 2013b). Notably, in the north-central Texas sections, the floral shift is documented over a stratigraphic interval of only 20 m, signaling the abruptness of this transition.

Conversely, Montañez et al. (2007, 2016) noted cyclical variability in pCO_2, as calculated from both the isotopic composition of pedogenic carbonate and stomatal indices of leaf fossils during the Desmoinesian, Missourian and the first half of Virgilian time. In their reconstruction, pCO_2 was relatively stable for an interval of ca. 3 Ma during most of the latter half of the Virgilian, before falling abruptly into the Wolfcampian. Notably, this interval of stability coincides with a significant long-term sea-level offlap, as recorded in the Donets Basin (Ukraine) (Montañez et al., 2016). Hence, we must consider the possibility that the entire Cutler Group exposure at Cañon del Cobre was deposited before the end of the Virgilian and does not extend into the Wolfcampian as thought. The vertebrate biostratigraphic record from the Cutler Group makes this supposition rather problematic, but the cross-correlation of the vertebrate record to marine biostratigraphy is frought with imprecision (e. g., Lucas, 2018) that makes it a possibility worth further investigation.

6.3. Causes of Wolfcampian climate change

As stated at the outset, numerous researchers have presented evidence including stable isotopes of pedogenic carbonate and phyllosilicates,

changing clay mineral assemblages (from kaolinitic to smectitic) and shifts from moist to xerophytic floral assemblages to suggest that a humid to sub-humid-seasonal climate prevailed during the latest Carboniferous (Gzhelian or Virgilian) at tropical latitudes, but was replaced during the earliest Permian (Asselian or Wolfcampian) by a more generally arid climate across central Pangea (Tabor and Montañez, 2002, 2004; Tabor et al., 2002, 2008; DiMichele et al., 2006; Cecil, 2013). DiMichele et al. (2009) highlight some of the difficulties in assigning a cause for the climatic shift at the Pennsylvanian-Permian boundary, including the approximate nature of many of the correlations between basins, and the varying environmental conditions across Pangea at the start of the transition. Peyser and Poulsen (2008) modeled the long-term shift in Carboniferous-Permian climate using a GCM and found widespread drying consistent with both deglaciation, due to a reduced latitudinal climate gradient and consequent decreased Hadley convection, and warming forced by increased pCO_2.

As described above, one explanation for the changing climate is the potential for pronounced reorganization of atmospheric circulation patterns during the initiation of the Pangean megamonsoon during the Pennsylvanian (Kutzbach and Gallimore, 1989; Parrish, 1993; Kutzbach and Ziegler, 1993; Gibbs et al., 2002; Tabor and Poulsen, 2008). Strong monsoonal atmospheric flow would have diverted the ITCZ away from the equatorial region toward the summer low at higher latitude, leading to tropical aridification (Tabor and Poulsen, 2008).

Significantly, a basinward shift in facies and/or a hiatus at the system boundary in many locations has been interpreted as a regression caused by the onset of a major episode of Gondwanan glaciation at this same time (Rygel et al., 2008). Notably, Montañez et al. (2007) utilized a combination of pedogenic carbonate $\delta^{13}C$ and fossil leaf stomatal data, supplemented by additional data in Montañez et al. (2016), to conclude that pCO_2 dropped sharply at the end-Virgilian from values of 400 to 600 ppm to a low of less than 200 ppm in the earliest Wolfcampian (early to mid-Asselian), before rising again in early Wolfcampian (late Asselian) time, continuing to rise in the Sakmarian. Montañez et al. (2007) cited brachiopod $\delta^{18}O$ data indicative of a cooling trend across the Carboniferous-Permian boundary in support of falling pCO_2. From the proxies, Montañez et al. (2016) concluded additionally that paleo-pCO_2 fluctuated with long eccentricity-scale timing (405 ka) until the mid-Virgilian, then stabilized until almost the end of the Virgillian, at which time pCO_2 fell. This decline, potentially reflecting late Paleozoic reorganization of forests and increased carbon sequestration, drove a cooling episode that caused the regrowth of Gondwanan ice sheets. Strong supporting evidence was provided by Davydov (2014), who used species counts of benthic foraminiferans as a proxy for water temperature on the shallow shelves of western tropical Pangea. This work documented a strong latest Pennsylvanian warming (late Gzhelian) followed by abrupt cooling at the system boundary.

Isbell et al. (2003) correlated the final major stage of Paleozoic glaciation as initiating during the mid-Stephanian and terminating mid-Sakmarian. Montañez et al. (2007) refined the timing somewhat to define the Asselian glaciation as initiating more precisely at the Gzhelian-Asselian boundary. The final termination of the Late Paleozoic Ice Age has been linked to CO_2-forced warming and possibly the northward drift of Pangea, but not until middle Permian time (Montañez et al., 2007; Montañez and Poulsen, 2013). Thus, the warming trend interpreted for the Virgilian-Wolfcampian boundary by previous research (e.g., Tabor and Montañez, 2002; Tabor et al., 2013a, b) would seem to be contra-indicated by the more recent proxy data for pCO_2, although increased aridity is not inconsistent with the cooler climate.

The earliest Permian (Asselian) is associated with glacially-driven marine off-lap (see data for Donetsk Basin in Fig. 2, Montañez et al., 2016). Thus, the drying trend may have been related in some part to the withdrawal of epeiric seas following an early Virgilian highstand by increasing the distance to the source of atmospheric moisture. Moreover, the projected drop of pCO_2 and consequent growth of the Gondwanan ice sheet would have had the effect of reducing temperature and atmospheric moisture, even in the tropics (Perlmutter and Matthews, 1989). Additionally, Perlmutter and Plotnick (2003) posited that increased continentality during sea level lowstands would have enhanced monsoonal flow, thereby increasing the diversion of the ITCZ and increasing tropical aridity. Thus, the isotopic enrichment (of $\delta^{18}O$) observed in the Cutler Group pedogenic carbonates, spanning the Virgilian to early Wolfcampian, could be explained as resulting from climatic drying coupled with withdrawal of the shallow Pennsylvanian seas. We note, however, that linking the observed isotopic and pedogenic evidence for climate change across the Virgillian-Wolfcampian boundary with the Asselian glaciation is problematic given our data suggesting stable pCO_2 at a time during which it is thought to have been in decline.

7. Conclusions

Calcareous paleosols occur throughout the stratigraphic section at Cañon del Cobre, which spans the Virgillian-Wolfcampian boundary. Paleosol types include calcic Protosols, Argillisols, calcic Argillisols, argillic Calcisols and Calcisols. Most calcretes in both the El Cobre Canyon and Arroyo del Agua formations are immature, Stage II, but more mature Stage III calcretes occur in argillic Calcisols and Calcisols in both formations. There is a stratigraphic trend toward more calcareous paleosols, slightly thicker and more mature paleosols in general, and more calcretes in the Arroyo del Agua Formation than in the underlying El Cobre Canyon Formation. Although this evidence suggests aridification, it is not by itself conclusive as the projected decrease in depositional gradient and sedimentation rate during Arroyo del Agua deposition also can explain these features.

Isotopic analysis of pedogenic carbonates from the Cutler Group supports the interpretation of early Permian drying as $\delta^{18}O$ values exhibit enrichment approximately at the formation boundary, consistent with an interpretation of drying. We note that the timing of the aridification in the Chama Basin is consistent with widespread regression forced by the onset of glaciation at the start of the Wolfcampian (Asselian). Conversely, we note also that the observed consistency of $\delta^{13}C$ values for the entire sampled section of the Cutler Group, which implies stable pCO_2 for this interval, is difficult to reconcile with the cooling that triggered the glaciation at this time.

Acknowledgments

We thank Karl Krainer for his research in the Cañon del Cobre that helped provide the stratigraphic framework used here. Additionally, we thank William DiMichele and an anonymous reviewer for insightful comments, and Brian Jones for editorial guidance in preparing the final version of the manuscript.

References

Allen, J.R.L., Wright, V.P., 1989. Paleosols in siliciclastic sequences. University of Reading, Postgraduate Research Institute of Sedimentology Short Course Notes, no. 1, p. 97.
Allison, G.B., Barnes, C.J., Hughes, M.W., Leaney, F.W.J., 1984. Effect of climate and vegetation on oxygen-18 and deuterium profiles in soils. Isotope Hydrology 1983: Proceedings of a Symposium, Vienna, 12–16 September 1983, pp. 105–123.
Alonso-Zarza, A.M., 2003. Palaeoenvironmental significance of palustrine carbonates and calcretes in the geological record. Earth-Science Reviews 60, 261–298.
Alonso-Zarza, A.M., Wright, V.P., 2010a. Palustrine carbonates. In: Alonso-Zarza, A.M., Tanner, L.H. (Eds.), Carbonates in Continental Environments: Processes, Facies and Applications. Developments in Sedimentology 61. Elsevier, Amsterdam, pp. 103–131.
Alonso-Zarza, A.M., Wright, V.P., 2010b. Calcretes. In: Alonso-Zarza, A.M., Tanner, L.H. (Eds.), Carbonates in Continental Environments: Processes, Facies and Applications. Developments in Sedimentology 61. Elsevier, Amsterdam, pp. 226–267.
Alonso-Zarza, A.M., Calvo, J., García del Cura, M.A., 1992. Palustrine sedimentation and associated features—grainification and pseudomicrokarst—in the Middle Miocene (intermediate unit) of the Madrid Basin, Spain. Sedimentary Geology 76, 43–61.
Armenteros, I., Daley, B., Garcia, E., 1997. Lacustrine and palustrine facies in the Bembridge Limestone (late Eocene, Hampshire Basin) of the Isle of Wight, southern England. Palaeogeography, Palaeoclimatology, Palaeoecology 128, 111–132.
Birkeland, P.W., 1999. Soils and Geomorphology. 3rd ed. Oxford, New York (536 pp.).

Cecil, C.C., 2003. The concept of autocyclic and allocyclic controls on sedimentation and stratigraphy, emphasizing the climatic variable. In: Blaine, C.C., Terence, E.N. (Eds.), Climate Controls on Stratigraphy. 77. SEPM Special Publication, Tulsa, pp. 13–20.
Cecil, C.C., 2013. An overview and interpretation of autocyclic and allocyclic processes and the accumulation of strata during the Pennsylvanian–Permian transition in the central Appalachian Basin, USA. International Journal of Coal Geology 119, 21–31.
Cecil, C.B., Dulong, F.T., West, R.R., Stamm, R., Wardlaw, B.A., Edgar, N.T., 2003. Climate controls on the stratigraphy of a Middle Pennsylvanian cyclothem in North America;. In: Blaine, C.C., Terence, E.N. (Eds.), Climate controls on stratigraphy. 77. SEPM Special Publication, Tulsa, pp. 151–182.
Davydov, V., 2014. Warmwater benthic foraminifera document the Pennsylvanian–Permian warming and cooling events — the record from the Western Pangea tropical shelves. Palaeogeography, Palaeoclimatology, Palaeoecology 414, 284–295.
DiMichele, W.A., Chaney, D.S., 2005. Pennsylvanian-Permian fossil floras from the Cutler Group, Cañon del Cobre and Arroyo del Agua areas, in northern New Mexico. New Mexico Museum of Natural History & Science Bulletin 31, 26–33.
DiMichele, W.A., Tabor, N.J., Chaney, D.S., 2005. Outcrop-scale environmental heterogeneity and vegetational complexity in the Permo-Carboniferous Markley Formation of North Central Texas. In: Lucas, S.G., Zeigler, K.E. (Eds.), The Nonmarine Permian. New Mexico Museum of Natural History and Science Bulletin 30, pp. 60–66.
DiMichele, W.A., Tabor, N.J., Chaney, D.S., Nelson, W.J., 2006. From wetlands to wet spots: environmental tracking and the fate of Carboniferous elements in Early Permian tropical floras. In: Greb, S.F., DiMichele, W.A. (Eds.), Wetlands Through Time. Geology Society of America, Special Paper 399, pp. 223–248.
DiMichele, W.A., Montañez, I.P., Poulsen, C.J., Tabor, N.J., 2009. Vegetation-climate feedbacks and regime shifts in the Late Paleozoic ice age earth. Geobiology 7, 200–226.
DiMichele, W.A., Chaney, D.S., Kerp, H., Lucas, S.G., 2010. Late Pennsylvanian floras in western equatorial Pangea, Cañon del Cobre, New Mexico. New Mexico Museum of Natural History & Science Bulletin 49, 75–133.
Dinterman, P.A., Mack, G.H., Leeder, M., Perez-Arlucea, M., 2000. Paleoclimatic control on Early Permian fluvial to eolian transition in New Mexico. Abstracts with Progam. Geology Society of America 32 (7), 254.
Dubiel, R.F., Blodgett, R.H., Bown, T.M., 1987. Lungfish burrows in the Upper Triassic Chinle and Dolores formations, Colorado Plateau. Journal of Sedimentary Petrology 57, 512–521.
Eberth, D.A., Miall, A.D., 1991. Stratigraphy, sedimentology and evolution of a vertebrate-bearing braided to anastomosed fluvial system, Cutler Formation (Permian-Pennsylvanian), north-central New Mexico. Sedimentary Geology 72, 225–252.
Ekart, D.D., Cerling, T.E., Montanez, I.P., Tabor, N.J., 1999. A 400 million-year carbon isotope record of pedogenic carbonate: implications for paleoatmospheric carbon dioxide. American Journal of Science 299, 805–827.
Esteban, M., Klappa, C.F., 1983. Subaerial exposure environments. In: Scholle, P.A., Bebout, D.G., Moore, C.H. (Eds.), Carbonate Depositional Environments. American Association of Petroleum Geologists, Memoir 33, p. 1296.
Fracasso, M.A., 1987. Fluvial deposition and paleoenvironment of the Cutler Formation red beds, El Cobre Canyon, New Mexico. New Mexico Geology 9, 14–25.
Freytet, P., Verrecchia, E.P., 2002. Lacustrine and palustrine carbonate petrography: an overview. Journal of Paleolimnology 27, 221–237.
Gat, J.R., 1996. Oxygen and hydrogen isotopes in the hydrologic cycle. Annual Review of Earth and Planetary Sciences 24, 225–262.
Gibbs, M.T., Rees, P.M., Kutzbach, J.E., Ziegler, A.M., Behling, P.J., Rowley, D.B., 2002. Simulations of Permian climate and comparisons with climate-sensitive sediments. Journal of Geology 110, 33–55.
Gile, L.H., Peterson, F.F., Grossman, R.B., 1966. Morphological and genetic sequences of accumulation in desert soils. Soil Science 100, 347–360.
Giles, J.M., Soreghan, M.J., Benison, K.C., Soreghan, G.S., Hasiotis, S.T., 2013. Lakes, loess, and paleosols in the Permian Wellington Formation of Oklahoma, U.S.A.: implications for paleoclimate and paleogeography of the Midcontinent. Journal of Sedimentary Research 83, 825–846.
Gradstein, F.M., Ogg, J.G., Schmitz, M., Ogg, G. (Eds.), 2012. The Geologic Time Scale 2012. vol. 2. Elsevier, Amsterdam (1175 pp.).
Hsieh, J.C.C., Chadwick, O.A., Kelly, E.F., Savind, S.M., 1998. Oxygen isotopic composition of soil water: quantifying evaporation and transpiration. Geoderma 82, 269–293.
Isbell, J.L., Miller, M.F., Wolfe, K.I., Lenaker, P.A., 2003. Timing of late Paleozoic glaciation in Gondwana: was glaciation responsible for the development of northern hemisphere cyclothems? In: Chan, M.A., Archer, A.W. (Eds.), Extreme Depositional Environments: Mega end Members in Geologic Time. Geology Society of America, Special Paper 370, pp. 5–24
Kempter, K., Zeigler, K., Koning, D., Lucas, S.G., 2007. Preliminary geologic map of the Canjilon SE quadrangle, Rio Arriba County, New Mexico. New Mexico Bureau of Geology and Mineral Resources Open-file Geologic Map 150, scale 1:24,000.
Kessler, J.L.P., Soreghan, G.S., Wacker, H.J., 2001. Equatorial aridity in western Pangea: Lower Permian loessite and dolomitic paleosols in northeastern New Mexico, USA. Journal of Sedimentary Research 71, 817–832.
Krainer, K., Lucas, S.G., 2010. Sedimentology of the Pennsylvanian-Permian Cutler Group and Lower Permian Abo Formation, Northern New Mexico. New Mexico Museum of Natural History & Science Bulletin 49, 25–36.
Kraus, M.J., 1999. Paleosols in clastic sedimentary rocks: their geologic applications. Earth Science Reviews 47, 41–70.
Kutzbach, J.E., Gallimore, R.G., 1989. Pangean climates: megamonsoons of the megacontinent. Journal of Geophysical Research 94, 3341–3357.
Kutzbach, J.E., Ziegler, A.M., 1993. Simulation of Late Permian climate and biomes with an atmosphere/ocean model: comparisons with observations. Philosophical Transactions of the Royal Society of London B 341, 327–340.
Lucas, S.G., 2018. Permian tetrapod biochronology, correlation and evolutionary events. In: Lucas, S.G., Shen, S.Z. (Eds.), The Permian timescale. Geological Society (London), Special Publication 450, pp. 405–444.
Lucas, S.G., Krainer, K., 2005a. Cutler Group (Permo-Carboniferous) stratigraphy, Chama Basin, New Mexico. New Mexico Museum of Natural History & Science Bulletin 31, 90–100.
Lucas, S.G., Krainer, K., 2005b. Stratigraphy and correlation of the Permo-Carboniferous Cutler Group, Chama Basin, New Mexico. New Mexico Geological Society Guidebook 56, 145–159.
Lucas, S.G., Spielmann, J.A., Krainer, K., 2010a. Summary of geology of Canon del Cobre, Rio Arriba County, New Mexico. New Mexico Museum of Natural History & Science Bulletin 49, 15–24.
Lucas, S.G., Harris, S.K., Spielmann, J.A., Rinehart, L.F., Berman, D.S., Henrici, A.C., Krainer, K., 2010b. Vertebrate paleontology, biostratigraphy and biochronology of the Pennsylvanian-Permian Cutler Group, Cañon del Cobre, northern New Mexico. New Mexico Museum of Natural History & Science Bulletin 49, 115–123.
Lucas, S.G., Krainer, K., DiMichele, W.A., Voigt, S., Berman, D.S., Henrici, A.C., Tanner, L.H., Chaney, D.S., Elrick, S.D., Nelson, W.J., Rinehart, L.F., 2015. Lithostratigraphy, biostratigraphy and sedimentology of the Upper Paleozoic Sangre de Cristo Formation, southwestern San Miguel County, New Mexico. New Mexico Geology Society Guidebook 66, 211–228.
Machette, M.N., 1985. Calcic soils of the southwestern United States. In: Weide, D.L. (Ed.), Soils and Quaternary Geology of the Southwest United States. Geological Society of America, Special Paper 203, pp. 1–21.
Mack, G.H., James, W.C., Monger, H.C., 1993. Classification of paleosols. Geological Society of America Bulletin 105, 129–136.
Mack, G.H., Leeder, M., Perez-Arlucca, M., Bailey, B., 2003. Early Permian silt-bed fluvial sedimentation in the Orogrande basin of the Ancestral Rocky Mountains, New Mexico, USA. Sedimentary Geology 160, 159–178.
Michel, L.A., Tabor, N.J., Montañez, I.P., Schmitz, M.D., Davydov, V.I., 2015. Chronostratigraphy and paleoclimatology of the Lodève Basin, France: evidence for a pan-tropical aridification event across the Carboniferous-Permian boundary. Palaeogeography, Palaeoclimatology, Palaeoecology 430, 118–131.
Montañez, I.P., Poulsen, C.J., 2013. The Late Paleozoic Ice Age: an evolving paradigm. Annual Reviews in Earth and Planetary Science 41, 629–656.
Montañez, I.P., Tabor, N.J., Niemeier, D., DiMichele, W.A., Frank, T.D., Fielding, C.R., Isbell, J.L., 2007. CO_2-forced climate and vegetation instability during late Paleozoic deglaciation. Science 315, 87–91.
Montañez, I.P., McElwain, J.C., Poulsen, C.J., White, J.D., DiMichele, W.A., Wilson, J.P., Griggs, G., Hren, M.T., 2016. Climate pCO_2 and terrestrial carbon cycle linkages during Late Palaeozoic glacial-interglacial cycles. Nature Geoscience 9, 824–831.
Mountney, N.P., 2006. Periodic accumulation and destruction of aeolian erg sequences in the Permian Cedar Mesa Sandstone, White Canyon, southern Utah, USA. Sedimentology 53, 789–823.
Mujal, E., Fortuny, J., Marmi, J., Dinarès-Turell, J., Bolet, A., Oms, O., 2018. Aridification across the Carboniferous–Permian transition in central equatorial Pangea: the Catalan Pyrenean succession (NE Iberian Peninsula). Sedimentary Geology 363, 48–68.
Parrish, J.T., 1993. Climate of the supercontinent Pangea. Journal of Geology 101, 215–253.
Perlmutter, M.A., Matthews, M.D., 1989. Global cyclostratigraphy: a model. In: Cross, T.A. (Ed.), Quantitative Dynamic Stratigraphy. Elsevier, Amsterdam, pp. 233–260.
Perlmutter, M.A., Plotnick, R.E., 2003. Hemispheric asymmetry of the marine stratigraphic record: conceptual proof of a unipolar ice cap. In: Cecil, C.B., Edgar, T.N. (Eds.), Climate Controls on Stratigraphy. Society of Economic Paleontologists and Mineralogists, Special Publication 77, pp. 51–66.
Peyser, C.E., Poulsen, C.J., 2008. Controls on Permo-Carboniferous precipitation over tropical Pangea: a GCM sensitivity study. Palaeogeography, Palaeoclimatology, Palaeoecology 268, 181–192.
Platt, N.H., 1989. Lacustrine carbonates and pedogenesis: sedimentology and origin of palustrine deposits from the Early Cretaceous Rupelo Formation, W Cameros Basin, N Spain. Sedimentology 36, 665–684.
Platt, N.H., 1992. Fresh-water carbonates from the lower Freshwater Molasse (Oligocene, western Switzerland): sedimentology and stable isotopes. Sedimentary Geology 78, 81–99.
Platt, N.H., Wright, V.P., 1992. Palustrine carbonates and the Florida Everglades: towards an exposure index for the fresh-water environment? Journal of Sedimentary Petrology 62, 1058–1071.
Plaziat, J.C., Freytet, P., 1978. Le pseudo-microkarst pédologique: un aspect particulier des paléo-pédogenèses développées sur les dépôts calcaires lacustres dans le tertiaire du Languedoc. Comptes Rendues Academie Science Paris 286, 1661–1664.
Retallack, G.J., 2001. Soils of the Past, 2d. Blackwell, Malden, MA, p. 404.
Retallack, G.J., 2005. Pedogenic carbonate proxies for amount and seasonality of precipitation in paleosols. Geology 33, 333–336.
Rygel, M.C., Fielding, C.R., Frank, T.D., Birgenheier, L.P., 2008. The magnitude of late Paleozoic glacioeustatic fluctuations: a synthesis. Journal of Sedimentary Research 78, 500–511.
Schaetzl, R.J., Thompson, M.L., 2015. Soils: Genesis and Geomorphology. 2nd ed. New York, Cambridge (777 pp.).
Schneider, J.W., Körner, F., Roscher, M., Kroner, U., 2006. Permian climate development in the northern peri-Tethys area - the Lodève basin, French Massif Central, compared in a European and global context. Palaeogeography, Palaeoclimatology, Palaeoecology 240, 161–183.
Smith, C.T., Budding, A.J., Pitrat, C.W., 1961. Geology of the southeastern part of the Chama basin. New Mexico Bureau of Mines and Mineral Resources Bulletin 75, 1–57.
Soreghan, G., Elmore, R., Lewchuck, M., 2002. Sedimentologic–magnetic record of western Pangean climate in upper Paleozoic loessite (lower Cutler beds, Utah). Geology Society of America Bulletin 114, 1019–1035.

Tabor, N.J., 2007. Permo-Pennsylvanian palaeotemperatures from Fe-oxide and phyllosilicate $\delta^{18}O$ values. Earth and Planetary Science Letters 253, 159–171.
Tabor, N.J., Montañez, I.P., 2002. Shifts in late Paleozoic atmospheric circulation over western equatorial Pangea: insights from pedogenic mineral $\delta^{18}O$ compositions. Geology 30 (12), 1127–1130.
Tabor, N.J., Montañez, I.P., 2004. Permo-Pennsylvanian alluvial paleosols (north-central Texas): high-resolution proxy records of the evolution of early Pangean paleoclimate. Sedimentology 51, 851–884.
Tabor, N.J., Montañez, I.P., 2005. Oxygen and hydrogen isotope compositions of pedogenic phyllosilicates: development of modern surface domain arrays and implications for paleotemperature reconstructions. Palaeogeography, Palaeoclimatology, Palaeoecology 223, 127–146.
Tabor, N.J., Poulsen, C.J., 2008. Palaeoclimate across the Late Pennsylvanian–Early Permian tropical palaeolatitudes: a review of climate indicators, their distribution, and relation to palaeophysiographic climate factors. Palaeogeography, Palaeoclimatology, Palaeoecology 268, 293–310.
Tabor, N.J., Montañez, I.P., Southard, R.J., 2002. Mineralogical and stable isotopic analysis of pedogenic proxies in Permo-Pennsylvanian paleosols: implications for paleoclimate and paleoatmospheric circulation. Geochimica et Cosmochimica Acta 66, 3093–3107.
Tabor, N.J., Montañez, I.P., Scotese, C.R., Poulsen, C.J., Mack, G.H., 2008. Paleosol archives of environmental and climatic history in paleotropical western Pangea during the latest Pennsylvanian through early Permian. Geology Society of America Special Paper 441, 291–303.
Tabor, N.J., Romanchock, C.M., Looy, C.V., Hotton, C.L., DiMichele, W.A., Chaney, D.S., 2013a. Conservatism of Late Pennsylvanian vegetation patterns during short-term and long-term directional environmental change, western equatorial Pangea. In: Gasiewicz, A., Slowakiewicz, M. (Eds.), Paleozoic Climate Cycles: Their Evolutionary and Sedimentological Impact. Geological Society, London, Special Publications 376, pp. 201–234.
Tabor, N.J., DiMichele, W.A., Montañez, I.P., Chaney, D.S., 2013b. Late Paleozoic continental warming of a cold tropical basin and floristic change in western Pangea. International Journal of Coal Geology 119, 177–186.
Talbot, M.R., 1990. A review of the paleohydrological interpretation of carbon and oxygen isotopic ratios in primary lacustrine carbonates. Chemical Geology 80, 261–279.
Talbot, M.R., Kelts, K., 1990. Paleolimnological signatures from carbon and oxygen isotopic ratios in carbonates from organic rich lacustrine sediments. In: Katz, B.J. (Ed.), Lacustrine Exploration: Case Studies and Modern Analogues. American Association of Petroleum Geologists, Memoir 50, pp. 99–112.
Tanner, L.H., 2000. Palustrine/lacustrine and alluvial facies of the Norian Owl Rock Formation (Chinle Group), Four Corners region, southwestern USA: implications for Late Triassic paleoclimate. Journal of Sedimentary Research 70 (5), 1280–1289.
Tanner, L.H., Lucas, S.G., 2007. Origin of sandstone casts in the Upper Triassic Zuni Mountains Formation, Fort Wingate, New Mexico. New Mexico Museum of Natural History and Science Bulletin 40, 209–214.
Tanner, L.H., Lucas, S.G., 2017. Paleosols of the Upper Paleozoic Sangre de Cristo Formation, north-central New Mexico: record of early Permian palaeoclimate in tropical Pangea. Journal of Palaeogeography 6 (2), 144–162.
Utting, J., Lucas, S.G., 2010. Palynological investigation of the Upper Pennsylvanian (Carboniferous) El Cobre Canyon Formation, Cutler Group, Canon del Cobre, Rio Arriba County, New Mexico, U.S.A. New Mexico Museum of Natural History and Science Bulletin 49, 71–73.
Zhu, L., Tabor, N.J., 2014. Lower Permian paleosol morphologies and paleoatmospheric pCO_2 estimates from north-central Texas, USA. Abstracts with Program. Geology Society of America 46 (6), 131.